energy&fuels

pubs.acs.org/EF
Article

Methane Hydrate Formation in the Presence of Magnetic Fields: Laboratory Studies and Molecular-Dynamics Simulations

Mengdi Pan,* Bastien Radola, Omid Saremi, Christopher C. R. Allen, and Niall J. English

Cite This: *Energy Fuels* 2024, 38, 23497−23506

ABSTRACT: One of the enigmas associated with natural gas hydrates relates to their formation and stabilization under certain conditions. Given the ubiquity of methane hydrates in marine sediments and permafrost milieus, their environmental significance is clear. In this paper, we provide a comprehensive investigation on the formation process of methane hydrates in the presence of magnetic fields of various strengths, given the already-established environmental performance of the Earth's magnetic field. Laboratory measurements were carried out with the support from molecular-dynamics simulations to glean insights into molecular scale mechanisms. Our findings revealed an inhibiting effect of magnetic fields on hydrate formation kinetics, which could be attributed to the strengthening of intermolecular interactions and the slowing of diffusion of water and methane molecules. The impact of magnetic fields appeared to be mostly kinetic in nature with little impact on hydrate stability. This clarification may offer a fresh perspective on the dynamics of liquid−solid transformation during the hydrate formation process, signaling critical interests in both natural and industrial applications.

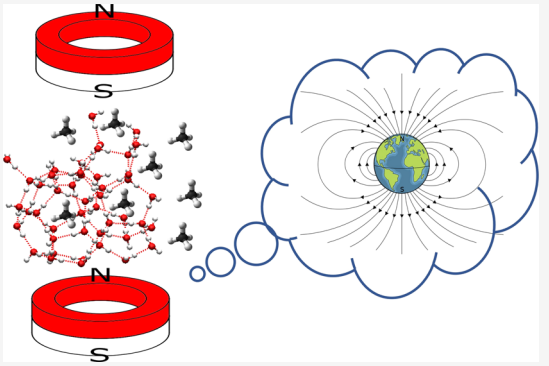

1. INTRODUCTION

Gas hydrates are crystalline, ice-like compounds in which hydrogen bonded water molecules form a three-dimensional framework of water cavities, which trap guest molecules.[1,2] Natural methane hydrates are widely distributed in marine sediments, permafrost areas, and deep lakes where low-temperature and high-pressure conditions prevail.[3,4] As a highly concentrated form of methane, it is considered as a promising energy resource and a possible climate-relevant factor. In recent decades, there has been raising awareness of the significance of methane released from the destabilization of hydrate deposits. Indeed, methane is a powerful greenhouse gas, even 84−86 times more potent over a 20-year period than CO_2.[5] Evidence from modeling studies indicates that the measurable growth and depletion of hydrate deposits over long geological time scales may result from environmental variations.[6] In turn, a massive methane release might have been a contributing agent to rapid global warming events such as the Paleocene−Eocene Thermal Maximum[7] and Quaternary glacial-to-interglacial transitions.[8] It is therefore crucial to investigate the hydrate formation kinetics, as well as the stability of existing hydrate deposits under specific circumstances.

The application of external magnetic fields has been proven to change the physicochemical properties of water or other aqueous solutions, such as an increase of viscosity,[9] an enhancement of vaporization,[10] changes in water structure,[11] changes in the contact angle at water/solid interface[12] and reduced surface tension.[13] These changes have been mainly associated with the modifications of hydrogen bond structuring.[14,15] Previous studies have also investigated the effects of magnetic fields on the crystallization behavior of different particles, such as calcium carbonate.[16−18] It turned out that the properties of the solution and the magnetic field strength both played a significant role, either promoting or inhibiting the formation of crystal nuclei.

Considering the aforementioned effects of external magnetic fields on water/solution properties and the crystallization process, there is little doubt that magnetic fields can manipulate hydrate formation. However, limited studies deal with this topic, and the impacts are still not straightforward. Makogon[19] first reported that magnetic fields may lead to the formation of denser hydrates with more regular structures. Liu et al.[20] explored the effects of magnetic fields on the formation of HCFC-141b refrigerant gas hydrates and reported a promoting effect with reduced induction time. This statement was supported by Shu et al.[21] who applied a rotating magnetic field on the same hydrate and found that the formation

Received: September 20, 2024
Revised: November 26, 2024
Accepted: November 27, 2024
Published: December 10, 2024

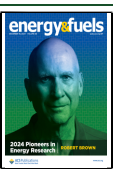

https://doi.org/10.1021/acs.energyfuels.4c04596
Energy Fuels 2024, 38, 23497−23506

temperature was also increased. A recent study on CO_2 hydrates also revealed a similar phenomenon in which the induction time was shortened while the gas consumption amount and rate were increased. In addition, the magnetic field thermodynamically promoted the formation of CO_2 hydrates by shifting the phase equilibrium to lower pressure and higher temperature conditions.[22] On the other hand, insignificant impacts on induction time, gas consumption, and pressure drop were observed on the kinetics of CO_2 hydrate formation when employing a magnetic field with an intensity of 55 mT.[23] Others have also suggested an inhibition effect with the presence of static magnetic fields on the thermodynamics of multicomponent gas hydrates (ranging from 0 to 400 mT)[24] and on the formation kinetics of methane hydrates (ranging from 0 to 95 mT).[25] Critically, it is hard to conclude from the literature whether an applied magnetic field alone promotes or inhibits hydrate formation under these conditions.

The Earth is surrounded by a magnetic field that is constantly changing, both in terms of its intensity and the gradual shifting or even complete inversion of the poles over geological time.[26] It is therefore possible to build a tentative link between the geomagnetic field and natural gas hydrate deposits, which has already been proposed as the "Belfast hypothesis". According to this hypothesis, changes in the Earth's magnetic field may influence methane hydrate deposits by affecting their stability, potentially releasing significant methane into the atmosphere during reversals. This release may contribute to climate events on geological time scales, like rapid warming or even mass extinctions.[27] Considering the ambiguous understanding of this topic, laboratory investigations were carried out in the present study to understand how the external static magnetic field in terms of strength and direction manipulates the methane hydrate formation process, in terms of both kinetics and thermodynamic properties. For an in-depth analysis of the mechanisms, molecular-dynamics simulations were also performed to help understand the principles of hydrate formation in the presence of magnetic fields. Discussions based on the experimental and simulation results reveal the effects of an external magnetic field on the hydrate formation process and provide greater insights into gas-hydrate formation. These findings may shed light on a further assessment of the evolution of natural gas hydrates.

2. METHODS

2.1. Experiments. Methane gas was acquired with a stated purity of 99.95% (BOC gases Ireland Limited). Milli-Q quality water was used for the formation of gas hydrates. The static magnets applied in the experiments are ring-sized N42 neodymium magnets with an outer diameter of 6 cm, an inner diameter of 4 cm, and a thickness of 0.5 cm (Magnet Expert Ltd.).

Methane gas hydrates were synthesized from water and methane gas in a high-pressure vessel made of 316 stainless steel with an internal volume of 340 cm^3. The overall scheme of the apparatus is demonstrated in Figure 1. The pressure inside the reactor was measured by a pressure transducer (G2, Ashcroft Inc.) with an uncertainty of 0.02 MPa, whereas a thermocouple (Parr Instrument Co.) with an accuracy of ±0.1 K was inserted directly into the water phase for the measurement of inner temperature. The temperature and pressure were recorded every second by a reactor controller (4838 reactor controller, Parr Instrument Company). The gas flow was regulated by a mass flow (EL-FLOW F-221M, Bronkhorst) that can be used at pressures up to 200 bar. For controlling the temperature in the system, the vessel was fitted in an aluminum jacket, which was cooled/heated by circulation of the cooling liquid from a cryostat (Julabo CF31). The magnetic field was induced by setting up

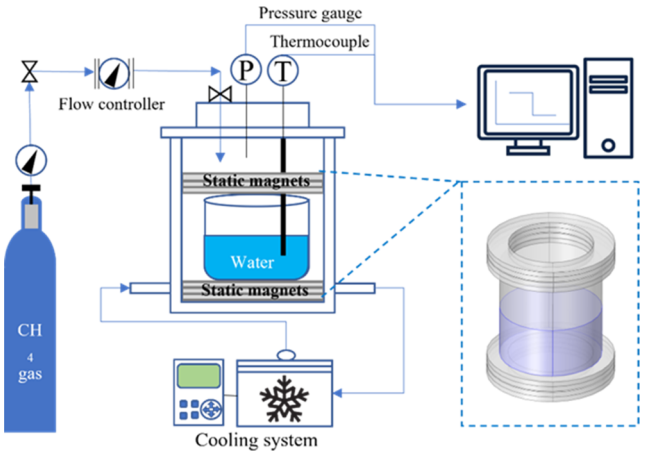

Figure 1. Technical sketch of the experimental setup.

the static N42 ring magnets on the top and bottom of the plastic jar in the reactor with their opposite poles facing each other (attracting forces). The selection of magnetic field strengths and configurations was based on prior literature and practical constraints of the setup, especially the handling limitations with neodymium magnets. Trials were carried out before the experiments with various configurations, including bar and ring magnets positioned either inside or outside the reactor. Preliminary results showed that placing ring magnets inside the reactor with a vertical field-vector direction offered greater stability and improved outcomes. Therefore, the different magnetic field configurations in this study were generated by changing the number of ring magnets inside the reactor and by switching the direction of the magnets. The magnetic field was characterized using the COMSOL software.[28]

For the determination of the hydrate formation kinetics, the plastic jar was initially filled with 30 mL of water and gently placed into the reactor with a certain number of static magnets being placed on the top and bottom of the jar (Figure 1). Since the magnetic stirrer was not applicable when testing the effects of magnetic fields, a limited amount of water was chosen after some tests to achieve as much hydrate conversion as possible. The reactor was carefully sealed and pressurized to 8 MPa with methane. It took less than 10 min for the temperature of the precooled system to reach the set point at 274 K. A pressure drop in the reactor indicated the formation of methane hydrates. In the temperature profile, a sudden increase was also observed due to the exothermic properties of the hydrate formation process. The system was kept at 274 K for 6 h to gauge a final steady state in which the pressure remained stable for more than 30 min. Based on the final pressure drop and thus the resulting moles of the consumed methane gas, we can roughly calculate the amount of hydrates formed over the experimental period on a mass-balance basis. Each test was repeated 4 times independently.

The hydrate equilibrium conditions with or without the presence of magnetic field were determined using the same setup based on the isochoric multistep method. Initially, the reactor was filled with 20 mL of water at 288 K and pressurized with methane at a desired pressure. The temperature was stabilized at 288 K for 15 min before it was cooled to 274 K within 20 min. The system was kept at 274 K for 4 h for the formation of methane hydrates. Thereafter, stepwise heating was adopted with the first step from 274 to 281 K within 30 min and the second step of slower heating to 288 K within the next 2.5 h to provide enough time for the system to reach an equilibrium state. By plotting the data of the pressure and temperature, the equilibrium condition was determined from the intersection between the slopes of cooling and heating under the selected pressure condition. Parallel tests were performed with 4 and 6 magnets in the reactor.

Gas hydrate formation kinetics was analyzed from the methane gas consumption in the sealed reactor which is calculated by the following equation (1)

https://doi.org/10.1021/acs.energyfuels.4c04596
Energy Fuels 2024, 38, 23497−23506

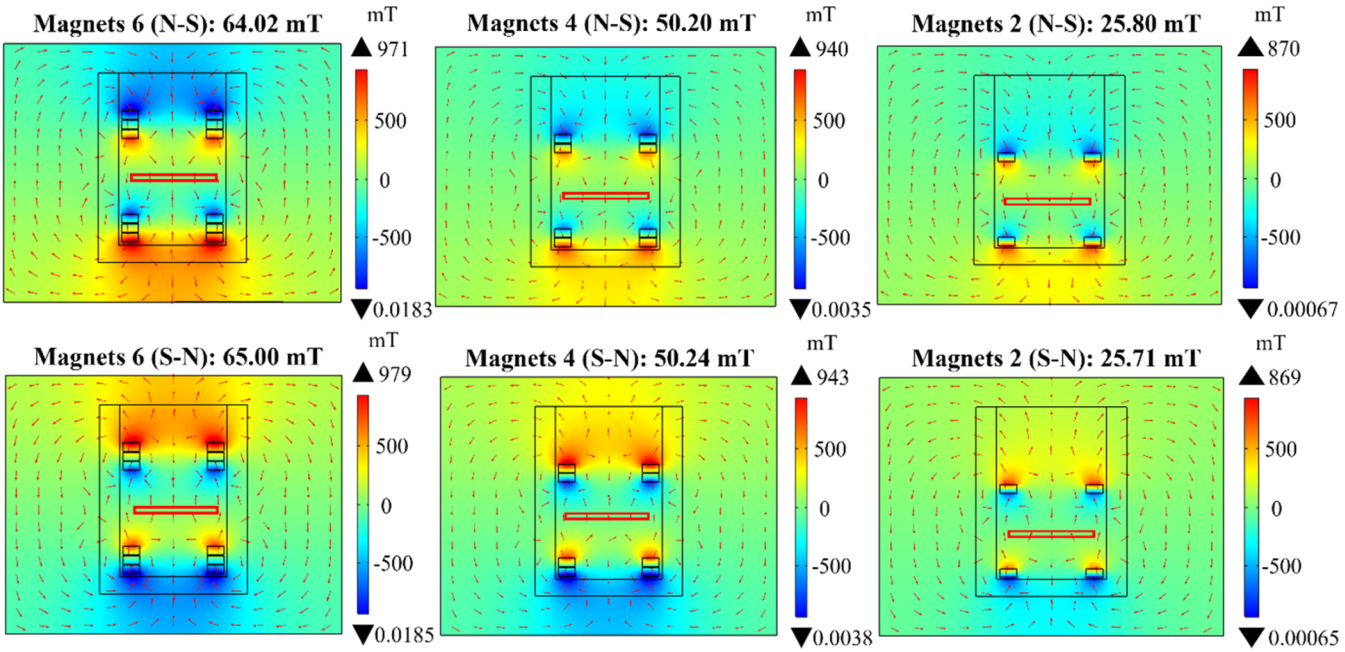

Figure 2. COMSOL-calculated contour plots of the total magnetic field intensity with red arrows indicating the field-vector direction and the color map representing field magnitude. The red rectangle demonstrates the gas–water interface area in the reactor. The black rectangles indicate the position and number of static N42 magnets applied in different configurations.

$$\Delta n_t = n_0 - n_t = \frac{p_0 V}{RTZ_0} - \frac{p_t V}{RTZ_t} \quad (1)$$

where, Δn_t is the quantity of methane gas consumed during the hydrate formation process after t min, n_0 and n_t are the quantity of methane gas in the reactor at 0 and t min, respectively. Correspondingly, p_0 and p_t represent the pressure in the reactor at 0 and t min. Z is the gas compressibility factor which is 0.85 calculating from the Standing–Katz chart of natural gas compressibility factors.[29] R is the universal gas constant, which, in this case, uses 8.314 J/(mol K). V is the volume of the methane gas, which should be the total volume of the reactor deducted by the volume of the occupied magnets and liquid. Given an ideal formula of methane hydrate, one mol of methane contains 5.75 mol of water with a molar mass (M_w) of 119.5 g. The gas hydrate density, ρ, is 0.91 g/cm^3. The hydrate formation rate is therefore determined from eq 2

$$v = \frac{\Delta n_t M_w}{t\rho} \quad (2)$$

where, v is the methane hydrate formation rate.

2.2. Molecular-Dynamics Simulations. Molecular-dynamics (MD) simulations were performed on a system composed of two distinct phases in contact: a methane hydrate crystal and a methane solution dissolved in liquid water. The simulation box was constructed as follows. First, a structure-I methane hydrate crystal measuring 48 × 48 × 48 Å^3 (i.e., 4 × 4 × 4 unit cells), containing 2944 water molecules and 512 methane molecules was created. Following the methodology of a previous study, the coordinates of oxygen atoms were taken from X-ray diffraction data[30] and the orientation of water molecules were randomly selected so as to follow Bernal–Fowler rules.[31] Then, the simulation box was extended to 144 Å (i.e., 3 times the size of the initial hydrate crystal) in the z direction, thus creating two interfaces in the xy plane. Incomplete hydrate cages at the interface were completed by the addition of water molecules. Finally, the empty space was filled with a liquid mixture of water and methane for a total of 7744 water and 896 methane molecules in the entire system. Note that the resulting methane–water ratio in the liquid phase was ∼8%, corresponding to supersaturated conditions. For the purpose of providing cleaner statistical analysis results, two additional systems were simulated under the same conditions: (a) a liquid system composed of a mixture of 3850 water molecules and 300 methane molecules in a 50 × 50 × 50 Å^3 box; and (b) a 48 × 48 × 48 Å^3 methane hydrate box containing 2944 water and 512 methane molecules. For the remainder of this paper, simulation results given for liquid alone and hydrate alone correspond to these two simpler systems, respectively.

The TIP4P/2005 general-purpose 4-site water model[32] was used alongside the OPLS-AA force field[33] for methane. Geometric combination rules were used to build cross-species interaction parameters, as recommended for OPLS. The cutoff distance for van der Waals interactions was set to 1.2 nm. Coulombic interactions were computed using the smooth particle mesh Ewald (SPME) scheme, with a relative error of 10^{-6}, to account for long-range contributions to the forces. The integration of the equations of movement was realized using the velocity Verlet algorithm with a time step of 2 fs. The simulations were performed in an isothermal–isobaric (NPT) ensemble at a temperature of 250 K and a pressure of 8 MPa. Note that while the pressure corresponded to the experimental conditions, the simulated temperature was adjusted to take account of the fact that the melting point of TIP4P/2005 water is lower than that of real water (i.e., ∼250 K versus 273.15 K).[34] The simulated thermodynamic conditions were within the stability zone for methane hydrate with the interaction potentials used. Together with the high methane content, the resulting high driving force towards hydrate formation allowed us to observe hydrate growth in reasonable simulation time. The temperature was kept constant using the Berendsen thermostat for equilibration runs, with a coupling constant τ_T = 0.1 ps, for a rapid relaxation of the temperature. For production runs, the Nosé–Hoover thermostat was used instead, with a coupling constant of τ_T = 0.5 ps. The pressure was similarly controlled using the semi-isotropic Berendsen barostat (τ_P = 0.5 ps) for equilibration runs, and the semi-isotropic Nosé–Hoover barostat (τ_P = 2 ps) for production runs.

Uniform magnetic fields of the form $\boldsymbol{B} = B\boldsymbol{e}_z$ were applied. Previous MD publications studying magnetic effects on aqueous solutions used B values in the range of 0–10 T and claimed a variety of impacts on structural and dynamic properties.[11,35,36] However, a recent paper convincingly showed that the Lorentz forces arising from such relatively weak magnetic fields are too small to have any statistically visible effects on MD results.[37] Indeed, the Lorentz forces are, under

https://doi.org/10.1021/acs.energyfuels.4c04596
Energy Fuels 2024, 38, 23497–23506

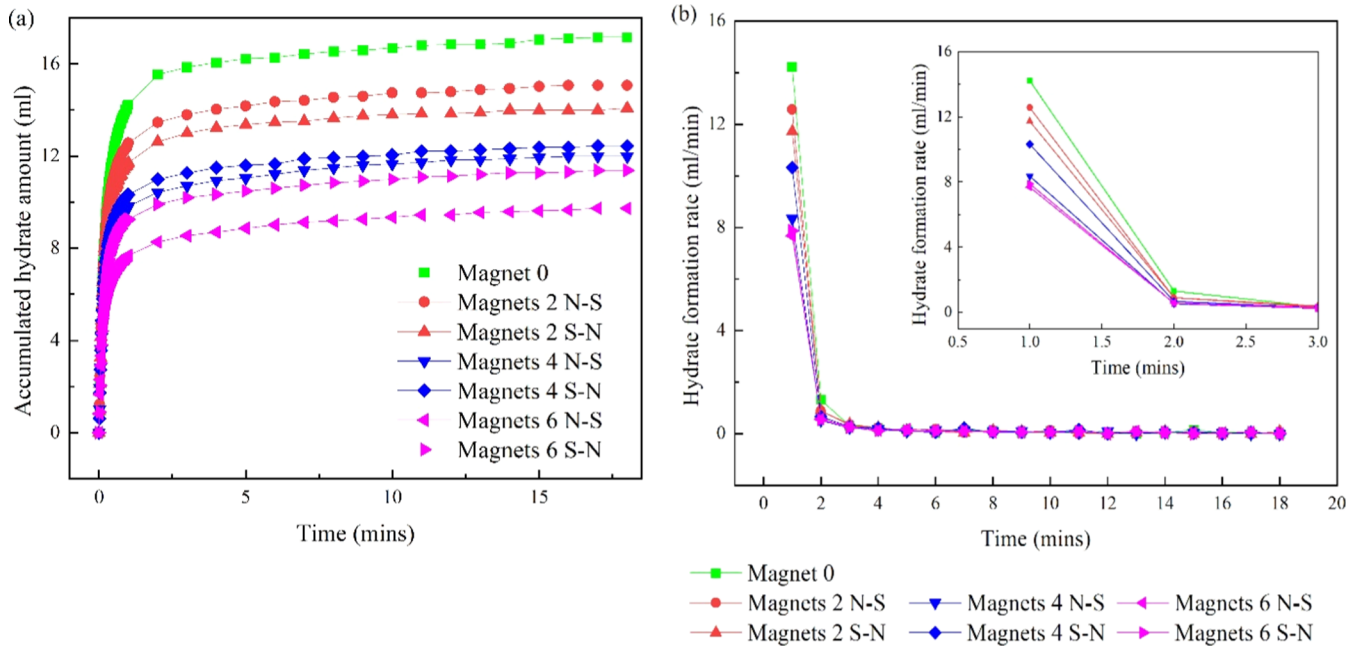

Figure 3. (a) Average accumulated amount of methane hydrate formed within the initial 18 min under different magnetic configurations in the 4 repetitive tests. (b) Average hydrate formation rate calculated for each minute within the initial 18 min.

these conditions, several orders of magnitude weaker than the intermolecular forces governing the dynamics of the system. In the same paper, the authors also argued that magnetic effects cancel out in classical MD and thus cannot be observed, but this position seems to stem from an incorrect derivation of the Hamiltonian of the system. Nevertheless, it is fair to say that the application of magnetic fields in classical simulations has become somewhat controversial. To the best of our knowledge, no other method is currently available to simulate magnetic effects in condensed matter systems. In this paper, we thus adopt the approach of increasing the simulated magnetic field strength for the Lorentz forces to reach a few percent of the intermolecular forces, so that the resulting perturbation can be detected and analyzed over short simulation times.[27] For our systems of interest, we found that magnetic field intensities of up to 1 MT were required to capture the full range of the physical response of the system. It should be emphasized that these unrealistic magnetic field strengths were not meant to correspond to real-life conditions and should be regarded as purely theoretical. Although the large differences in magnetic intensities prevented a direct comparison with laboratory measurements, simulations could nevertheless provide valuable insights into supporting the results of practical experiments.

For the larger system composed of a hydrate phase and a liquid phase, 1 ns-long equilibration runs were performed followed by 20 ns-long production runs. For the smaller liquid-only and hydrate-only systems, both equilibration and production run durations were set to 5 ns. Atomic positions, velocities, and forces were recorded every 10 ps for analysis. All simulations were performed using the DL_POLY 4.07 software package.[38]

3. RESULTS

3.1. Experimental Results. *3.1.1. Magnetic Field Characterization.* A magnetic field was generated from permanent N42 Neodymium magnets. Different configurations of the magnetic field were obtained by varying the number of magnets and shifting the direction of the magnetic poles. For a more precise and repeatable investigation, the specific magnetic field was simulated in COMSOL[28] and the magnetic field strength was calculated from the software (Figure 2). It should be mentioned that the direction of the magnetic field was designated as N−S if the magnetic field vector was from top to bottom, whereas S−N indicated the magnetic field direction was from bottom to top. It is clear that with the increasing number of magnets, the field strength also improved significantly as shown in Figure 2. However, there is no linear correlation between these two parameters. The direction of the magnetic vector seems to have only a minor effect on the resulting field strength.

3.1.2. Gas Hydrate Formation Kinetics. A series of experiments have been performed to investigate the methane hydrate formation process with the presence and absence of a magnetic field, regarding the formation rate and gas consumption. Figure 3a depicts the accumulated average hydrate amount formed within the first 18 min from repeated tests under various magnetic field configurations. It should be mentioned that time 0 was chosen after the system reached the hydrate stability zone. A dramatic increase was detected within the initial 2 min for all groups, indicating rapid hydrate formation after gas dissolution. Thereafter, the upward trend slowed down and gradually became steady. In the absence of a magnetic field, the highest amount of hydrate formation was observed, with magnetic field strength showing a negative correlation with accumulated hydrate quantity. Interestingly, Figure 3a shows a slight difference in hydrate formation between the N−S and S−N field orientations, especially in the group with 6 magnets where the N−S field orientation group reported a lower hydrate amount at the end of the experiment.

As indicated by the slope of the accumulated hydrate amount in Figure 3a, the hydrate formation rate with/without magnetic field was calculated for each minute (Figure 3b). The formation rate peaked at the first minute of the experiments under all magnetic field configurations. The figure shows a remarkable decrease over the course of the process, with hydrate formation almost coming to a halt after 10 min. This suggests that the system was approaching equilibrium at the end of the experiments. Similarly, the highest formation rate was obtained in the absence of a magnetic field. An increase in the field strength resulted in a reduction in the hydrate

https://doi.org/10.1021/acs.energyfuels.4c04596
Energy Fuels 2024, 38, 23497−23506

formation rate regardless of the magnetic field direction. Even though the experiment lasted for 6 h in each run, most of the hydrates were formed in the first 2 min. After the initial formation of the hydrate layer at the gas−water interface, subsequent formation was slowed down as gas molecules had to diffuse through the existing hydrate layer, a process which was rate-limiting. Therefore, an inhibition effect of the magnetic field on the hydrate formation kinetics can be inferred from the results.

The relationship between the magnetic field configuration and total gas consumption throughout the experiments is shown in Figure 4. Methane gas consumption in the absence of magnetic fields was higher than any other groups, reaching around 3.11 L. The inhibition effects of the magnetic field were again confirmed as the total gas consumption decreased with the increasing field strength. The lowest level of gas consumption, around 1.88 L, was detected for the group with 6 magnets, exhibiting a field strength of 65 mT. Notably, those magnetic configurations with the vectors from top to bottom (N−S) had larger variations as compared to those with vectors from bottom to top (S−N).

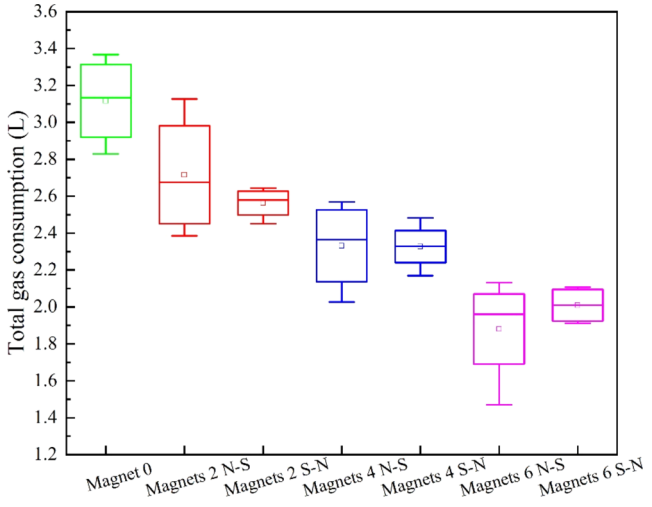

Figure 4. Total methane gas consumption during the whole experimental period (6 h) under different magnetic field configurations.

Due to the limitations of the experimental techniques, it is challenging to speculate about the mechanisms driving the inhibition of magnetic fields on methane hydrate formation kinetics. We therefore employed MD simulations to reveal the interactions between magnetic fields and methane hydrates on a molecular scale. Even though on a varying scale, the simulation results shown in Section 3.2 may intuitively provide insights into the observed unique phenomenon, offering a clear understanding of the role of magnetic fields in the hydrate formation process.

3.1.3. Gas Hydrate Thermodynamic Behavior. The gas hydrate equilibrium condition was determined using the isochoric method, based on a cooling/heating cycle at a constant volume. To improve the measurement accuracy, the hydrate equilibrium condition was first investigated without a magnetic field. The results were compared with those from published data[39] and thermodynamic models CSMGem[3] and PVTSim (Calsep, Denmark). Our experimental results (blue triangles in Figure 5a) obtained with pressures ranging from 3.0 to 9.5 MPa were generally in good agreement with the calculated data from these two models or literature data, especially for the measurements taken under lower pressure conditions, supporting the reliability of the experimental method.

The experimental results with 4 and 6 magnets are presented in Figure 5b. In the presence of a magnetic field, the equilibrium temperature of methane hydrates was slightly higher under the lower pressure conditions by about 1−2 K. As for the high-pressure conditions (above 60 bar), weaker effects were observed in the presence of a magnetic field. In other words, magnetic fields slightly promoted the formation of methane hydrates at lower pressure conditions by shifting the equilibrium curve to higher temperatures under identical pressures. This highlights the dual role of magnetic fields as a kinetic inhibitor and a thermodynamic promoter.

3.2. MD Simulation Results. The number of molecules in the hydrate phase were computed using the Baéz−Clancy criteria.[40] Results are given in Figure 6 as a function of simulation time. At the beginning of the runs, 60% of methane molecules are part of the hydrate phase. In the absence of a

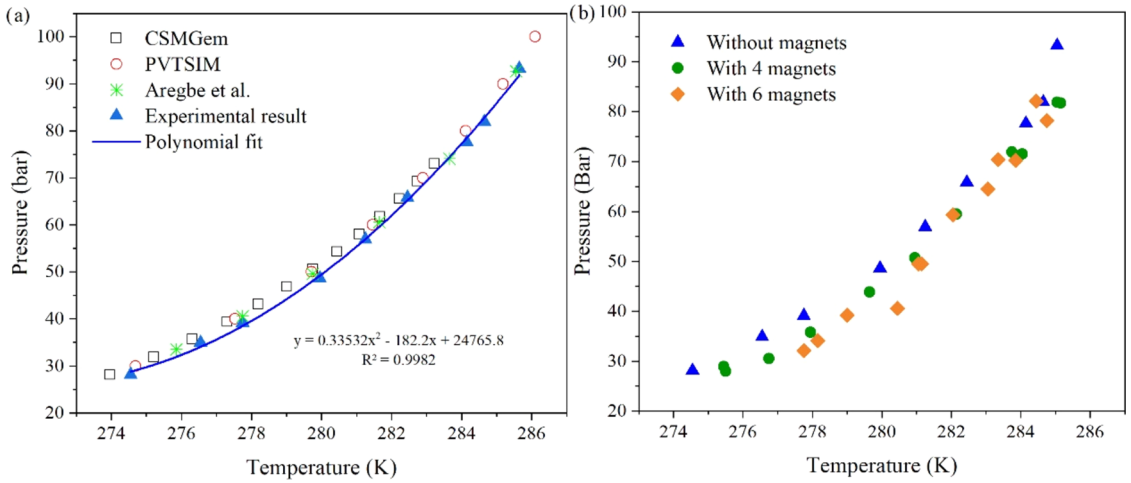

Figure 5. (a) Comparison of methane hydrate stability conditions from literature data, thermodynamic model calculations, and this study without magnetic field; (b) methane hydrate equilibrium $p-T$ conditions under various magnetic field strengths in this study.

https://doi.org/10.1021/acs.energyfuels.4c04596
Energy Fuels 2024, 38, 23497−23506

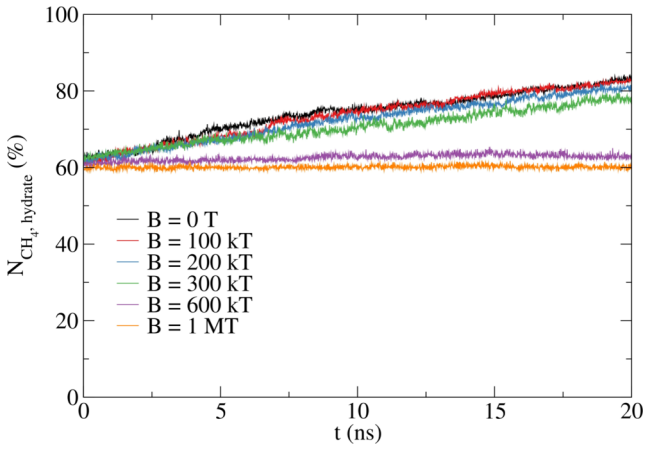

Figure 6. Evolution of the percentage of guest (methane) molecules in the hydrate phase as a function of simulation time at different values of the magnetic field intensity.

magnetic field, the percentage steadily grows to reach 82% after 20 ns. The presence of a magnetic field results in a decrease of the hydrate formation rate up to an almost total inhibition in the upper range of simulated field strengths (≥600 kT). At a lower field strength (100 kT), the magnetic effect is indiscernible over the course of the trajectory. Longer simulation times would be required to observe any inhibitory effect at this field strength or lower.

To analyze the intermolecular interactions in the systems, binding energy distributions between molecules *X*−*Y* were computed, where *X* and *Y* stand for either water or methane. The distributions were evaluated with respect to molecules *X*, so as to represent the interaction energy of each molecule of species *X* with all molecules of species *Y*. Binding energies for liquid and hydrate phases were computed on separate systems to emphasize the different response of the two phases when subjected to magnetic fields (Figure 7). The results show that water−water interactions in the liquid phase are slightly strengthened by a magnetic field. More precisely, the distributions become narrower around the average value of −100 kJ/mol, which corresponds to the energy of 4 hydrogen bonds for TIP4*P*/2005 water. This would suggest that magnetic effects increase the proportion of 4 hydrogen bonded water molecules at the expense of weaker 2 or 3 hydrogen bond structures. This is confirmed by the direct calculation of hydrogen bond distributions (not shown). Methane−water interactions in the liquid phase are likewise strengthened. Distributions become narrower and shift from −16 to −19 kJ/mol at 1 MT. In the hydrate phase, water−water interactions are also shown to be increased, but this effect tends to broaden the distributions instead, the left peak being shifted from −150 kJ/mol at low magnetic intensities to −200 kJ/mol at 1 MT. Likewise, methane-water interactions also exhibit strong magnetic effects at high field strengths which manifest themselves by the separation of two peaks, around −16 and −40 kJ/mol, respectively. These two peaks, which are barely discernible at lower field strengths, correspond to the two different types of cages of structure-I hydrates. Magnetic effects thus strengthen and tighten the hydrate crystal structure in a very significant way at high simulated magnetic intensities. Note that methane−methane interactions (not shown) are essentially zero in all cases due to the dissolved nature of methane in the systems considered here.

Radial distribution functions (RDF) between water molecules were computed separately for the liquid and the hydrate to shed light on the structural effects of magnetic field exposure (Figure 8). For the liquid, RDF peaks become slightly narrower with the magnetic field. Thus, the liquid water structure becomes slightly more orderly due to magnetic effects, which is consistent with the binding energy distributions and the changes in the hydrogen bond network discussed above. In the hydrate case, the effect is similar and long-range peaks (r > 7 Å), which are indiscernible at low field strengths, become apparent at high magnetic field intensities (≥600 kT). Again, this supports the interpretation of the binding energy distributions as a result of a tighter crystal structure at high field strengths.

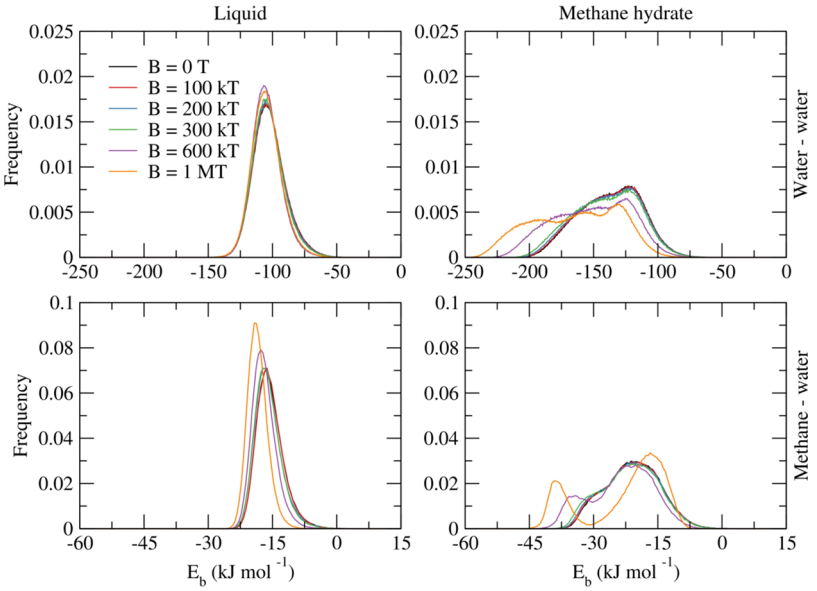

Figure 7. Binding energy distributions for (top) water−water and (bottom) methane-water interactions in (left) the liquid and (right) the methane hydrate. The colored curves correspond to different values of the magnetic field intensity.

https://doi.org/10.1021/acs.energyfuels.4c04596
Energy Fuels 2024, 38, 23497−23506

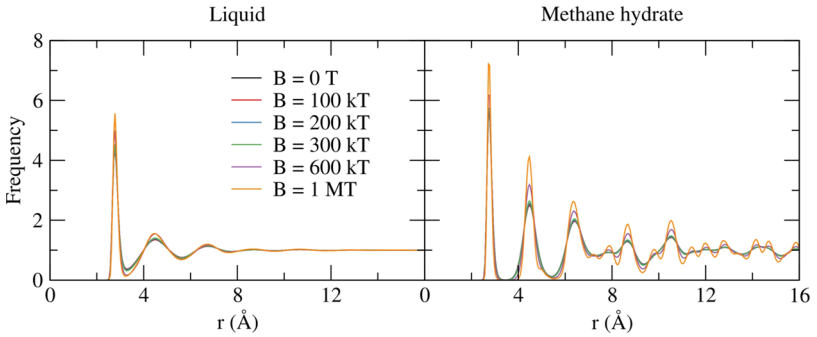

Figure 8. Radial distribution functions of water molecules for (left) the liquid and (right) methane hydrate. The colored curves correspond to different values of the magnetic field intensity.

Diffusion coefficients in the liquid phase were evaluated from the mean squared displacements (MSD) using the Einstein's relation

$$\lim_{t\to\infty} \langle |r(t) - r(0)|^2 \rangle = 6Dt \tag{3}$$

with the notation $\langle \cdots \rangle$ denoting an average over all molecules and over different starting origins (Figure 9). In the absence of a magnetic field, the diffusivity at the simulated thermodynamic conditions and for the interaction potentials used is 11.7 Å^2 ns^{-1} for water molecules and 9.7 Å^2 ns^{-1} for methane molecules. The lower mobility of methane molecules is consistent with their bigger effective size compared to that of water molecules. Magnetic fields significantly slow the diffusive dynamics of both molecular species. From 0 to 100 kT, the diffusion coefficient decreases by 9.3% for water and by 3.0% for methane. This trend accelerates for field strengths up to 1 MT, where the diffusivity is 0.07 Å^2 ns^{-1} for water and 0.05 Å^2 ns^{-1} for methane: a 99.4 and 99.5% decrease, respectively. Overall, the diffusivity for both species is impacted by magnetic fields in a similar way, both qualitatively and quantitatively.

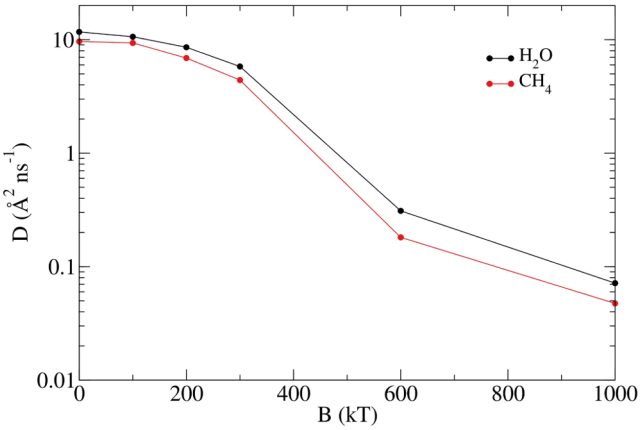

Figure 9. Diffusion coefficients for water and methane molecules in the liquid phase as a function of the magnetic field strength. Lines connecting the data points are guides for the eye only. Error bars, estimated from the linear fits of the MSD, are too small to be visible on the graph and are therefore omitted.

4. DISCUSSION

Considering the experimentally observed variations in the hydrate formation kinetics and thermodynamic properties in the presence and absence of magnetic fields, it is crucial to investigate the hydrate formation process at the molecular level. Gas hydrate formation is a phase transition process and mainly consists of two stages: nucleation and growth.[41] At the molecular scale, water and gas molecules may first form half-cage hydrate structures, serving as nucleation centers. After reaching a critical size, the hydrate growth process starts.[42] Reaction kinetics, heat transfer, and mass transfer are the main controlling mechanisms postulated for hydrate growth.[42]

In our experiments, gas hydrates were mainly formed within the first 2 min. It can be speculated that right after pressurization gas molecules were dissolved in the liquid phase up to supersaturation, thus starting the hydrate formation process. With the consumption of both water and gas molecules, the rate of hydrate formation gradually decreased. At the end of the hydrate formation process, the limitation of mass/heat transfer may result in a lower hydrate formation rate as compared to the control. The key parameter in this study was the application of magnetic fields, which impacted hydrate formation rate, gas consumption, as well as thermodynamic properties in different test groups. It is likely that the properties of water and the interaction between molecules during nucleation and growth are influenced by magnetic fields. The observed difference between the test groups with N−S and S−N field orientations may suggest that the dynamics of molecules at the gas−water interface were influenced by the magnetic field direction, especially at a higher magnetic field strength (6 magnets). Also, a larger variation was detected in the results with N−S field orientation, which might indicate that the N−S configuration aligns more effectively with the gravitational vector in the reactor, causing more fluctuations in the orientation of the molecules and hydrogen bonding near the interface. However, further research is needed to fully understand how the reversed magnetic field direction impacts hydrate formation, as the underlying mechanisms remain complex and not yet fully elucidated.

MD simulation results supported the inhibitory effect of magnetic fields on hydrate formation primarily through kinetic rather than thermodynamic effects, which were consistent with the experimental observations. In the lower range of simulated magnetic intensities (<600 kT), magnetic effects slightly strengthened the interactions and slightly tightened the structure of both the liquid and the hydrate phases, suggesting that thermodynamic effects on hydrate growth might be rather weak at these field strengths. At higher field intensities (≥600 kT), magnetic effects had a much more pronounced impact on the hydrate phase, both in terms of structure and energetics, compared to the effects observed on the liquid. With respect to

https://doi.org/10.1021/acs.energyfuels.4c04596
Energy Fuels 2024, 38, 23497−23506

hydrate formation, however, it is unclear if the relative strengthening of the gas hydrate energetics and structure compared to the liquid would have a promoting or an inhibitory effect. Nevertheless, one key observation in the simulation was the visible increase of the methane−water interaction energies in the liquid phase under magnetic fields, which could enhance mixing and, thus, theoretically promote hydrate nucleation. This particular mechanism could potentially explain the slight thermodynamic promoting effect observed experimentally. A thorough thermodynamic study would be required to confirm any influence on hydrate stability in the MD simulations. However, due to the large number of pressure and temperature conditions that would need to be probed with extended simulation times, this would unfortunately exceed our limited computational resources. Overall, the thermodynamic effects of magnetic fields appear quite weak and do not explain the inhibitory effect observed in hydrate formation kinetics. At the same time, the diffusion of water and methane molecules was reduced by magnetic fields, resulting in increasingly viscous dynamics as the field strength increased. Consequently, the enclathration of gas molecules into the well-structured hydrate cavities were slowed down by the magnetic effects, thus inhibiting hydrate formation kinetics. It should be stressed that, although simulation results appear consistent with experimental observations, we must be wary of being overconfident in the ability of simulations to account for the mechanisms at play. Indeed, as already discussed in Section 2.2, simulating magnetic effects is a difficult task, and due to the high simulated magnetic intensities compared to laboratory conditions, direct comparison with experiments should be treated with caution. In particular, it is unclear if threshold effects occur at very high field strengths, influencing simulation results in a way that more realistic magnetic fields would not. Further research would be needed to confirm the molecular-scale mechanisms suggested by the present simulation results.

It should be noted that not all magnetic field configurations necessarily lead to changes in the hydrate formation process.[20,23] The magnetic effect, either promotion or inhibition, is highly dependent on the solution properties and field strength.[18,43] This may somehow explain the contrasted statements about the effects of magnetic fields on hydrate formation. Specifically, the inhibition effects of magnetic fields on hydrate formation, whether kinetic or thermodynamic, has been underpinned by the decrease in the surface tension of water, the weakening of hydrogen bonds, and the disruption of cage arrangements.[24,25,44−46] Nevertheless, others interpreted that magnetic fields decrease the contact angle between water and solid surface and reduce the hydrate nucleation size and free energy, thus promoting heat transfer and hydrate formation.[12,21,22,47] In another research, it was found that the presence of a magnetic field significantly promoted the formation of CO_2 hydrates. However, instead of a direct effect of the magnetic field on gas/water molecules, the impact was attributed to the magnetic properties of the presented Fe_3O_4 nanoparticles, which acted as nucleation sites and improved the heat transfer for hydrate formation.[48] In light of these limited studies on this topic, which have tended to focus on experimental observations or isolated numerical simulations; the conclusions may be deemed not comprehensive. This is where our study lies, as an effective integration of laboratory experiments with supporting MD simulations, conducting independent analysis on various scales.

The overall findings of this study illustrate an inhibitory effect of magnetic fields on methane hydrate formation. This could add an intriguing dimension to the "Belfast hypothesis", which proposed a tentative link between the effects of reversals of the Earth's magnetic field on the release of methane trapped in gas hydrates and, consequently, its possible contribution to mass extinction events.[27] Indeed, while our results support only a slight thermodynamic stabilization of methane hydrates in the presence of a magnetic field, they may suggest some kind of kinetic stabilization. In other words, changes in the Earth's magnetic field could help stabilize hydrate deposits against environmental changes that are expected to occur over geological time scales.

5. CONCLUSIONS

In this study, we have investigated the effects of externally applied magnetic fields on methane hydrate formation using lab experiments with additional supporting numerical simulations. Static magnetic fields were controlled by shifting the number of magnets, including their reversals in the direction. Experimental results have shown that the application of magnetic fields kinetically inhibits the formation of methane hydrates while slightly increasing hydrate stability. Simulation results were qualitatively satisfied with these observations and could potentially be used to improve our understanding of hydrate formation mechanisms. In particular, they suggested that intermolecular interactions might be strengthened by magnetic fields, and the water structure might be tightened. Meanwhile, a decrease in the diffusivity of water and methane molecules was also observed in the simulations. Even though the energetic and structural properties of the hydrate and liquid phases were modified by magnetic fields, the inhibitory effect on hydrate formation did not appear to be influenced by this in any significant way. Instead, the inhibitory effect appeared to be mostly kinetic in nature, resulting in slowed dynamics in the liquid.

■ ASSOCIATED CONTENT

Data Availability Statement

Data available on request from the authors.

■ AUTHOR INFORMATION

Corresponding Author

Mengdi Pan − *School of Chemical and Bioprocess Engineering, University College Dublin, Belfield D04 V1W8, Ireland;* orcid.org/0000-0003-0632-1799; Email: mengdi.pan@ucd.ie

Authors

Bastien Radola − *School of Chemical and Bioprocess Engineering, University College Dublin, Belfield D04 V1W8, Ireland; School of Biological Sciences, Queen's University Belfast, Belfast BT9 5DL Northern Ireland, U.K.;* orcid.org/0000-0002-6232-0814

Omid Saremi − *School of Chemical and Bioprocess Engineering, University College Dublin, Belfield D04 V1W8, Ireland*

Christopher C. R. Allen − *School of Biological Sciences, Queen's University Belfast, Belfast BT9 5DL Northern Ireland, U.K.*

Niall J. English − *School of Chemical and Bioprocess Engineering, University College Dublin, Belfield D04 V1W8, Ireland;* orcid.org/0000-0002-8460-3540

https://doi.org/10.1021/acs.energyfuels.4c04596
Energy Fuels 2024, 38, 23497−23506

Complete contact information is available at:
https://pubs.acs.org/10.1021/acs.energyfuels.4c04596

Author Contributions

M.P.: Conceptualization, methodology, experimental investigation, data curation, writing—original draft, writing—reviewing and editing. B.R.: Conceptualization, methodology, simulation analysis, data curation, writing—original draft, writing—reviewing and editing. O.S.: Methodology, investigation. C.C.R.A.: Conceptualization, supervision, funding acquisition, writing—reviewing and editing. N.J.E.: Conceptualization, supervision, funding acquisition, writing—reviewing and editing.

Notes

The authors declare no competing financial interest.

■ ACKNOWLEDGMENTS

This research was supported by Leverhulme Trust Research Project Grant under the grant number RPG-2021-243. Mengdi Pan, Niall English, and Omid Saremi are grateful for valuable advice from Mohammad Reza Ghaani in designing some experiments.

■ REFERENCES

(1) Stackelberg, M. V. Feste Gashydrate. *Naturwissenschaften* **1949**, *36*, 327−333.
(2) Müller, H. R.; von; Stackelberg, M. Zur Struktur der Gashydrate: 2. Mitteilung. *Naturwissenschaften* **1952**, *39*, 20−21.
(3) Sloan, E. D.; Koh, C. A. *Clathrate Hydrates of Natural Gases*, 3rdrd ed.; CRC Press Taylor and Francis Group: Boca Raton, FL, USA, 2008.
(4) Kvenvolden, K. A. Gas hydrates—geological perspective and global change. *Rev. Geophys.* **1993**, *31*, 173−187.
(5) Intergovernmental Panel on Climate Change (IPCC). In *Climate Change 2013: The Physical Science Basis. Contribution of Working Group I to the Fifth Assessment Report of the Intergovernmental Panel on Climate Change*; Cambridge University Press: Cambridge, U.K. and New York, 2013.
(6) Haacke, R. R.; Westbrook, G. K.; Riley, M. S. Controls on the formation and stability of gas hydrate-related bottom-simulating reflectors (BSRs): A case study from the west Svalbard continental slope. *J. Geophys. Res.: Solid Earth* **2008**, *113*, No. B05104.
(7) Dickens, G. R.; Oneil, J. R.; Rea, D. K.; Owen, R. M. Dissociation of Oceanic Methane Hydrate as a Cause of the Carbon Isotope Excursion at the end of the Paleocene. *Paleoceanography* **1995**, *10*, 965−971.
(8) Kennett, J. P.; Cannariato, K. G.; Hendy, C. H. *Methane Hydrates in Quaternary Climate Change: The Clathrate Gun Hypothesis, Washington D C* 2003.
(9) Ghauri, S. A.; Ansari, M. S. Increase of water viscosity under the influence of magnetic field. *J. Appl. Phys.* **2006**, *100*, No. 066101.
(10) Nakagawa, J.; Hirota, N.; Kitazawa, K.; Shoda, M. Magnetic field enhancement of water vaporization. *J. Appl. Phys.* **1999**, *86*, 2923.
(11) Chang, K.-T.; Weng, C.-I. The effect of an external magnetic field on the structure of liquid water using molecular dynamics simulation. *J. Appl. Phys.* **2006**, *100*, 1802.
(12) Otsuka, I.; Ozeki, S. Does magnetic treatment of water change its properties? *J. Phys. Chem. B* **2006**, *110*, 1509−1512.
(13) Zhan, X.; Zhu, Z.; Sun, D. W. Effects of extremely low frequency electromagnetic field on the freezing processes of two liquid systems. *LWT* **2019**, *103*, 212−221.
(14) Cai, R.; Yang, H.; He, J.; Zhu, W. The effects of magnetic fields on water molecular hydrogen bonds. *J. Mol. Struct.* **2009**, *938*, 15−19.
(15) Inaba, H.; Saitou, T.; Tozaki, K. I.; Hayashi, H. Effect of the magnetic field on the melting transition of H2O and D2O measured by a high resolution and supersensitive differential scanning calorimeter. *J. Appl. Phys.* **2004**, *96*, 6127−6132.
(16) Zhao, Y.; Zhang, X.; Xu, X.; Zhang, S. Research progress in nucleation and supercooling induced by phase change materials. *J. Energy Storage* **2020**, *27*, No. 101156.
(17) Higashitani, K.; Kage, A.; Katamura, S.; Imai, K.; Hatade, S. Effects of a Magnetic Field on the Formation of CaCO3 Particles. *J. Colloid Interface Sci.* **1993**, *156*, 90−95.
(18) Jha, P. K.; Xanthakis, E.; Jury, V.; Le-Bail, A. An Overview on Magnetic Field and Electric Field Interactions with Ice Crystallisation; Application in the Case of Frozen Food. *Crystals* **2017**, *7*, 299.
(19) Makogon, Y. F. *Hydrates of Hydrocarbons*; Pennwell Books: UK, 1997.
(20) Liu, Y.; Guo, K.; Liang, D.; Fan, S. Effects of magnetic fields on HCFC-141b refrigerant gas hydrate formation. *Sci. China, Ser. B:Chem.* **2003**, *46*, 407−415.
(21) Shu, B.; Ma, X.; Guo, K.; Li, J. Influences of different types of magnetic fields on HCFC-141b gas hydrate formation processes. *Sci. China, Ser. B:Chem.* **2004**, *47*, 428−433.
(22) Sun, S.; Li, Y.; Gu, L.; Yang, Z.; Zhao, J. Experimental study on carbon dioxide hydrate formation in the presence of static magnetic field. *J. Chem. Thermodyn.* **2022**, *170*, No. 106764.
(23) Moeini, H.; Bonyadi, M.; Esmaeilzadeh, F.; Rasoolzadeh, A. Experimental study of sodium chloride aqueous solution effect on the kinetic parameters of carbon dioxide hydrate formation in the presence/absence of magnetic field. *J. Nat. Gas Sci. Eng.* **2018**, *50*, 231−239.
(24) Mohammad, B.; Madani Tehrani, D. Effect of magnetic field on gas hydrate formation. *Nat. Gas Ind. B* **2022**, *9*, 240−245.
(25) Ghaani, M. R.; English, N. J.; Allen, C. C. R. Magnetic-Field Manipulation of Naturally Occurring Microbial Chiral Peptides to Regulate Gas-Hydrate Formation. *J. Phys. Chem. Lett.* **2020**, *11*, 9079−9085.
(26) Bloxham, J.; Gubbins, D. The Evolution of the Earth ' s Magnetic Field. *Sci. Am.* **1989**, *261*, 68−75.
(27) English, N. J.; Allen, C. C. R. Magnetic-field effects on methane-hydrate kinetics and potential geophysical implications: Insights from non-equilibrium molecular dynamics. *Sci. Total Environ.* **2019**, *661*, 664−669.
(28) COMSOL AB. COMSOL Multiphysics v. 5.4.S n.d. www.comsol.com.
(29) Wang, Y.; Ye, J.; Wu, S. An accurate correlation for calculating natural gas compressibility factors under a wide range of pressure conditions. *Energy Rep.* **2022**, *8*, 130−137.
(30) McMullan, R. K.; Jeffrey, G. A. Polyhedral Clathrate Hydrates. IX. Structure of Ethylene Oxide Hydrate. *J. Chem. Phys.* **1965**, *42*, 2725−2732.
(31) Bernal, J. D.; Fowler, R. H. A Theory of Water and Ionic Solution, with Particular Reference to Hydrogen and Hydroxyl Ions. *J. Chem. Phys.* **1933**, *1*, 515−548.
(32) Abascal, J. L. F.; Vega, C. A general purpose model for the condensed phases of water: TIP4P/2005. *J. Chem. Phys.* **2005**, *123*, 234505 DOI: 10.1063/1.2121687.
(33) Jorgensen, W. L.; Maxwell, D. S.; Tirado-Rives, J. Development and testing of the OPLS all-atom force field on conformational energetics and properties of organic liquids. *J. Am. Chem. Soc.* **1996**, *118*, 11225−11236.
(34) Blazquez, S.; Vega, C. Melting points of water models: Current situation. *J. Chem. Phys.* **2022**, *156*, No. 216101.
(35) Wang, J.; Lin, H.; An, S.; Li, S.; Li, F.; Yuan, J. Concentration-dependent structure of KCl aqueous solutions under weak magnetic field from the X-ray diffraction and molecular dynamics simulation. *J. Mol. Struct.* **2020**, *1201*, No. 127130.
(36) Moosavi, F.; Gholizadeh, M. Magnetic effects on the solvent properties investigated by molecular dynamics simulation. *J. Magn. Magn. Mater.* **2014**, *354*, 239−247.
(37) Panczyk, T.; Camp, P. J. Lorentz forces induced by a static magnetic field have negligible effects on results from classical

molecular dynamics simulations of aqueous solutions. *J. Mol. Liq.* **2021**, *330*, No. 115701.
(38) Todorov, I. T.; Smith, W.; Trachenko, K.; Dove, M. T. DL_POLY_3: new dimensions in molecular dynamics simulations via massive parallelism. *J. Mater. Chem.* **2006**, *16*, 1911−1918.
(39) Aregbe, A. G.; Sun, B.; Chen, L. Methane Hydrate Dissociation Conditions in High-Concentration NaCl/KCl/CaCl 2 Aqueous Solution: Experiment and Correlation. *J. Chem. Eng. Data* **2019**, *64*, 2929−2939.
(40) BÁEZ, L. A.; Clancy, P. Computer Simulation of the Crystal Growth and Dissolution of Natural Gas Hydratesa. *Ann. N.Y. Acad. Sci.* **1994**, *715*, 177−186.
(41) Schicks, J. M. Gas Hydrates: Formation, Structures, and Properties. In *Hydrocarb. Oils Lipids Divers. Orig. Chem. Fate*; Wilkes, H., Ed.; Springer, 2018; pp 1−15.
(42) Christiansen, R. L.; Dendy Sloan, E. Mechanisms and Kinetics of Hydrate Formation. *Ann. N. Y. Acad. Sci.* **1994**, *715*, 283−305.
(43) Dalvi-Isfahan, M.; Hamdami, N.; Xanthakis, E.; Le-Bail, A. Review on the control of ice nucleation by ultrasound waves, electric and magnetic fields. *J. Food Eng.* **2017**, *195*, 222−234.
(44) Wang, Q.; Li, L.; Chen, G.; Yang, Y. Effects of magnetic field on the sol-gel transition of methylcellulose in water. *Carbohydr. Polym.* **2007**, *70*, 345−349.
(45) Zhao, L.; Ma, K.; Yang, Z. Changes of Water Hydrogen Bond Network with Different Externalities. *Int. J. Mol. Sci.* **2015**, *16*, 8454−8489.
(46) Su, N.; Wu, C. F. Effect of magnetic field treated water on mortar and concrete containing fly ash. *Cem. Concr. Compos.* **2003**, *25*, 681−688.
(47) Pang, X. F.; Bo, D. The changes of macroscopic features and microscopic structures of water under influence of magnetic field. *Phys. B* **2008**, *403*, 3571−3577.
(48) Firoozabadi, S. R.; Bonyadi, M.; Lashanizadegan, A. Experimental investigation of Fe3O4 nanoparticles effect on the carbon dioxide hydrate formation in the presence of magnetic field. *J. Nat. Gas Sci. Eng.* **2018**, *59*, 374−386.

https://doi.org/10.1021/acs.energyfuels.4c04596
Energy Fuels 2024, 38, 23497−23506